AIChE

Nonuniform Channels in Adsorbent Monoliths

B. D. Crittenden, O. Camus, S. P. Perera, T. J. Mays, and F. Sánchez-Liarte
Dept. of Chemical Engineering, University of Bath, Bath BA2 7AY, U.K.

S. R. Tennison, and E. Crezee
MAST Carbon Technology Ltd., Henley Park, Guildford, Surrey GU3 2AF, U.K.

DOI 10.1002/aic.12335
Published online July 20, 2010 in Wiley Online Library (wileyonlinelibrary.com).

A model is introduced to account for nonuniform channel geometries in monolithic adsorbents. Based on nonisothermal operation, fully developed parabolic flow and the full three-dimensional convection-diffusion equation, the model is applied to the adsorption of dichloromethane from an air stream flowing through a binder-less activated carbon monolith. The equilibrium parameters and the effective diffusion coefficient for adsorption are obtained independently from gravimetric adsorption experiments. The nonuniform channel model is capable of predicting breakthrough curves as a function of feed gas flow rates up to dimensionless breakthrough concentrations of about 0.4–0.6, depending on the feed flow rate. Even though the variation of effective diffusion coefficient with both concentration and temperature has been tested, successful prediction over the whole range of concentration may require the incorporation of further aspects relating to the anisotropic nature of the carbon. © 2010 American Institute of Chemical Engineers *AIChE J,* 57: 1163–1172, 2011
Keywords: activated carbon monoliths, channel modeling, nonuniformities, VOC control

Introduction

Activated carbon monoliths are structured, low pressure drop materials which show excellent potential in environmental control applications such as the recovery of volatile organic compounds from air streams.[1] Carbon-based monolithic adsorbents can be of coated or integral types. Carbon-coated monoliths have been prepared (i) by dip-coating ceramic monoliths in a polymer mixture with subsequent carbonization and activation,[2] (ii) by extrusion of commercial activated carbon using a polymer as a binder,[3] and (iii) by growth of carbon filaments over deposited metal particles on a ceramic surface.[4] Integral monoliths have been prepared (i) by extrusion of a carbon-binder mixture,[5,6] and (ii) by the extrusion of phenolic resins followed by carbonization and activation to create a binder-less activated carbon monolith.[7]

Correspondence concerning this article should be addressed to O. Camus at O.Camus@bath.ac.uk.

The binder-less route provides a greater density of the active adsorbent and allows the carbon pore structure to be controlled precisely. Equally important, the binder-less monolith provides a uniform electrical resistance which can be exploited in its thermal regeneration step in a thermal swing adsorption process.[8] Electrical regeneration facilitates a much faster cycle time, and hence, the cost of the adsorption process can be reduced considerably compared with conventional packed beds that require medium temperature steam or hot inert gas for the regeneration of the carbon.[1] The binder-less activated carbon monolith has been shown to compare favorably in performance with granular material[9] and to be capable of providing a more sustainable route for the control and recovery of volatile organic compounds.[10,11]

In the simplest approach, monolith design can be based on the performance of an individual channel making the assumption that all the channels are identical. It is possible to use the height equivalent to a theoretical plate (HETP) methodology[12] which Ahn and Brandani[13] improved by developing a 3D model and establishing a simple HETP

Table 1. Physical Properties of Carbon Monolith

Monolith overall length, L_m	103 mm
Monolith overall diameter, d_m	18.6 mm
Monolith total mass	13.2 g
Nominal channel size, $d_{ch} = 2a$	0.70 mm
Nominal wall thickness, $e = 2t_w$	0.35 mm
Fractional free cross-section, $\varepsilon = \frac{d_{ch}^2}{(d_{ch}+e)^2}$	0.44

equation to take into account the effect of the solid material in the four corners of the monolith wall. Ahn and Brandani[14] considered the nonuniformity of both the channel size and the wall thickness to obtain an excellent match for the adsorption of carbon dioxide on square channel carbon monoliths. There can be little doubt that variations from channel to channel are likely in a monolithic adsorbent since the pressure drop distribution measured through different channels of a monolith at constant flow rate could be described by a normal distribution.[15]

Because of advances in computing capacity and in numerical techniques to solve complex problems, 3-D models have been developed recently for adsorption in zeolite monoliths[16] or in thin zeolite films supported on a monolith.[17] A model has also been developed using Comsol Multiphysics™ to describe the complete adsorption-desorption cycle of an electric-swing adsorption system.[18] However, all these models are limited to single channel modeling and require the estimation of some of the model parameters to fit the experimental data. The purpose of this article, therefore, is to consider how the fundamental three-dimensional flow, energy, and adsorption equations can be used to account for the overall performance of an activated carbon monolith which has channels of varying dimensions that map onto a normal distribution. The model predictions are compared with experimental data obtained using the adsorption of dichloromethane (DCM) from air onto a research sample of a binderless monolith supplied by MAST Carbon Technology (Guildford, UK). The parameters of the model are obtained from independent measurements of the carbon monolith characteristics.

Materials and Experimental Method

Experimental dynamic breakthrough curves were obtained by the adsorption of DCM onto a square channel activated carbon monolith with a cell density of about 90 cells cm^{-2} (Table 1). To make this monolith, extruded phenolic resin was carbonized by heating in flowing nitrogen at 1 K min^{-1} to 1073 K with a dwell time of 1 h at this maximum temperature. The monolith was subsequently activated in flowing carbon dioxide for 8 h at 1123 K, whereby an activation level (weight loss) of 23.6% was achieved. The monolith was dried and weighed before insertion into a stainless steel column. As shown in Figure 1, a stream of air was bubbled through liquid DCM and then diluted with a further air stream to provide a feed concentration of about 2000 ppmv of DCM (Table 2). The air flow rates were controlled by float rotameters. A by-pass column filled with glass beads was used to measure the feed concentration before the adsorption experiment commenced. The outlet concentration from the monolith was monitored every 30 s using a flame

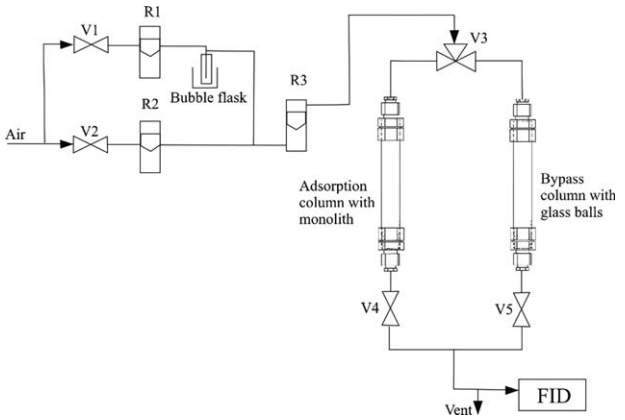

Figure 1. Schematic of adsorption experimental rig.

ionization detector and the data transferred to a computer. The adsorption experiments were performed at room temperature and because of minor variations in this temperature, slight variations in the DCM feed concentration were observed from run to run. Nonetheless, the analysis which follows will assume that more-or-less the same feed concentration was used in the three runs shown in Table 2. Prior to each experiment, the monolith was regenerated for 90 min at 483 K under a 0.25 L (STP) min^{-1} flow of nitrogen.

The average channel velocities u_{ave} shown in Table 2 were calculated by dividing the volumetric flow rate (measured at ambient conditions) by the free cross-sectional area of the monolith. The hydraulic mean diameter for a regular square channel with the nominal dimensions shown in Table 1 and the physical properties of air (since the DCM concentration was low) were used in the calculation of the Reynolds number.

Modeling

Ahn and Brandani[13] neglected the axial component of diffusion in the solid and represented the corners of the adsorbent structure as a separate domain. Even with these restrictions, the numerical solution was only obtained after several hours of simulation. In the present work, diffusion in the solid phase is considered in all three dimensions. It has also been possible to define a single domain for the solid phase as shown in Figure 2.

The solid domain is considered to be isotropic and equilibrium is assumed to exist at the interface between the gas channel and the monolith surface as the mass transfer zone passes down the channel. Extensive three-dimensional modeling of the channel flow has shown that there is very little difference in the breakthrough curves for the following three channel gas flow assumptions: (i) developing three-dimensional

Table 2. Experimental Conditions

Flow rate (L (STP) min^{-1})	Feed concentration, c_0 (ppmv)	Channel gas velocity, u_{ave} (m s^{-1})	Reynolds Number
5	1950	0.697	30.8
7	2000	0.976	43.1
9	1910	1.255	55.4

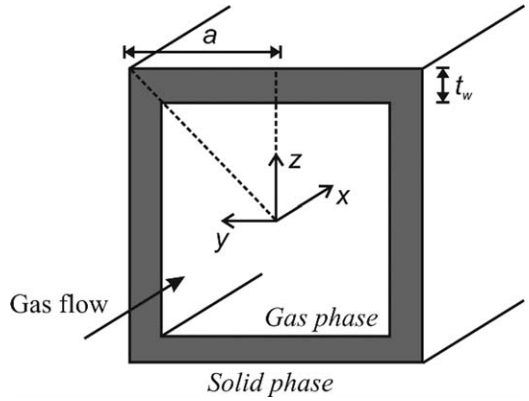

Figure 2. Schematic of a single square channel.

flow, (ii) fully developed three-dimensional flow, and (iii) plug flow. The expression for fully developed laminar flow in a rectangular duct was established by Cornish.[19] For a flow between two infinite parallel plates, this can be reduced to:

$$u = \frac{3}{2}u_{\text{ave}}\left(1 - \frac{y^2}{a^2}\right) \tag{1}$$

where u is the channel velocity along the y-axis. For reasons of symmetry in a square channel the velocity profile in the z-direction can be reduced to a similar expression. Thus, the parabolic velocity profile for a square channel can be approximated as follows:

$$u(y,z) = \frac{9}{4}u_{\text{ave}}\left(1 - \frac{y^2}{a^2}\right)\left(1 - \frac{z^2}{a^2}\right) \tag{2}$$

As shown in Figure 3, this expression is a good approximation of Cornish's exact solution of fully developed laminar flow.

Figure 4 shows the breakthrough curves obtained using the three channel flow models for a 7 L (STP) min^{-1} flow rate. It was ensured that the average velocities were identical in the comparison. The curves for developing flow and fully developed parabolic flow are actually coincident. However, the curve using the plug flow approximation reveals a longer time to the initial breakthrough than the other two. For industrial applications, the time to breakthrough is an important parameter in the design of adsorption units. Hence, in consideration of this aspect and for simplicity in developing the nonuniform channel model (NUCM), the fully developed parabolic flow assumption has been used in this study. This renders the channel flow model fully three-dimensional in terms of the gas phase concentration and thereby to be of the axially dispersed fully developed flow convection and diffusion type as shown in Eq. 3.

$$\frac{\partial c}{\partial t} - D_{\text{M}}\left(\frac{\partial^2 c}{\partial x^2} + \frac{\partial^2 c}{\partial y^2} + \frac{\partial^2 c}{\partial z^2}\right) + u(y,z)\left(\frac{\partial c}{\partial x} + \frac{\partial c}{\partial y} + \frac{\partial c}{\partial z}\right) = 0 \tag{3}$$

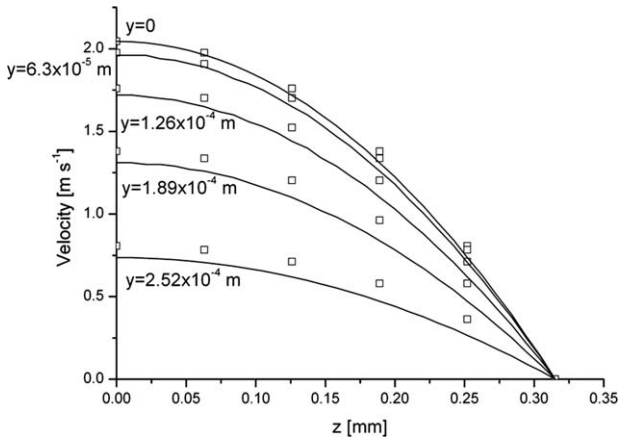

Figure 3. Comparison of parabolic velocity profile (lines) with Cornish's exact solution (squares).

Using an empirical equation provided by Fuller et al.[20] D_{M}, the molecular diffusion coefficient of DCM in air at 298 K and 101 kPa was calculated to be 1.05×10^{-5} m^2 s^{-1}. Diffusion of adsorbed DCM in the solid phase was represented by an effective diffusion coefficient D_{eff}:

$$\frac{\partial q}{\partial t} = D_{\text{eff}}\left(\frac{\partial^2 q}{\partial x^2} + \frac{\partial^2 q}{\partial y^2} + \frac{\partial^2 q}{\partial z^2}\right) \tag{4}$$

Here, q is the amount adsorbed. The rate of adsorption into the solid has been approximated using the linear driving force expression:

$$\frac{d\bar{q}}{dt} = k(q^* - \bar{q}) \tag{5}$$

in which $\bar{q}$ represents the average loading in the solid and q^* the surface concentration at equilibrium with the fluid phase. In an earlier study, the mass transfer coefficient k for various channel shapes was expressed in terms of geometric

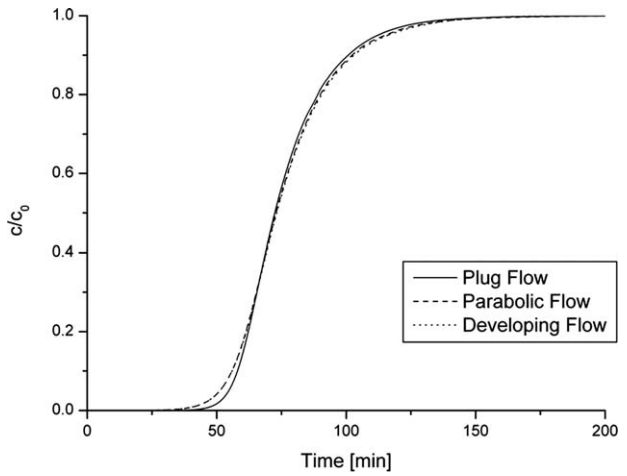

Figure 4. Breakthrough curves for the plug flow, parabolic flow and developing flow models.

transformation into an equivalent tubular geometry.[21] For a square channel, the mass transfer in a hollow channel insulated at the outer surface is given by:

$$k = \frac{4D_{\text{eff}}}{\left[\left(1-\frac{r_i}{r_o}\right)\left(r_o^2-r_i^2\right)-\frac{1}{r_o(r_o-r_i)}\left(\frac{1}{2}\left(r_o^4-r_i^4\right)-\frac{4r_i}{3}\left(r_o^3-r_i^3\right)+r_i^2\left(r_o^2-r_i^2\right)\right)\right]} \tag{6}$$

Here, r_o and r_i are the external and internal diameters, respectively, of the equivalent cylindrical channel. They are related to the channel dimensions as follows:

$$r_i = \frac{2d_{ch}}{t_w} \quad \text{and} \quad r_o = \sqrt{\frac{4t_w}{\pi}(t+d_{ch})+r_i^2} \tag{7}$$

From many gravimetric adsorption measurements made using an Intelligent Gravimetric Analyser IGA-001 (Hiden Isochema, Warrington, UK), the equilibrium between the DCM and samples of the activated carbon monolith has been found to be best described by the Tóth adsorption isotherm as shown in Figure 5:

$$q = q_{\max}\frac{b(T)p}{\left(1+(b(T)p)^t\right)^{1/t}} \tag{8}$$

Here, p is the partial pressure of DCM, $q_{\max}$ is the adsorption capacity (maximum amount adsorbed), t is the Tóth parameter and $b(T)$ is the affinity coefficient which is dependent on the absolute temperature by the van't Hoff equation:

$$b(T) = b_0 \exp\left(\frac{-\Delta H}{RT}\right) \tag{9}$$

From nonlinear regression analysis, the Tóth isotherm parameters were found to be: $q_{\max} = 4505$ mol m^{-3} and $b_0 = 1.06 \times 10^{-9}$ Pa^{-1}. The isosteric heat of adsorption was found to be $\Delta H = 46.2$ kJ mol^{-1}.

It is possible to reduce the computational time in the solution to the flow and concentration equations by considering four axes of symmetry, thereby reducing the element size to 1/8 of the channel, as shown in the top left corner of Figure 2. Many boundary conditions are required to solve the dynamics of the breakthrough.

Continuity of mass flux at the fluid-solid interfaces:

$$D_{\text{eff}}\left.\frac{\partial q}{\partial z}\right|_{z=a^+} = D_M\left.\frac{\partial c}{\partial z}\right|_{z=a^-} = \frac{d\bar{q}}{dt} \quad \text{for } 0<y<a \tag{10}$$

The parameters a^- and a^+ represent the spatial coordinates of the gas-solid interface in the gas and in the solid, respectively. Continuity of mass flux at the solid-solid interfaces is given by:

$$\left.\frac{\partial q}{\partial y}\right|_{y=0^+} = 0 \quad \text{for } a<z<a+t_w \tag{11}$$

$$\left.\left(\frac{\partial q}{\partial y}+\frac{\partial q}{\partial z}\right)\right|_{y=z} = 0 \quad \text{for } a<z<a+t_w \tag{12}$$

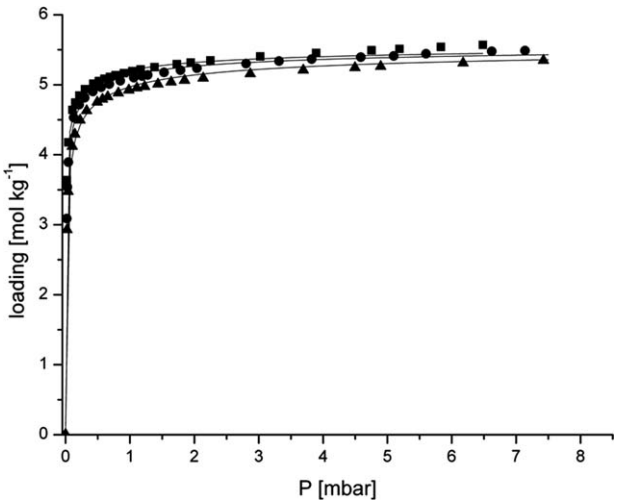

Figure 5. Adsorption isotherms of DCM on activated carbon monolith samples at 5 (■), 10 (●) and 20°C (▲) described by the Tóth expression (solid lines).

$$\left.\frac{\partial q}{\partial z}\right|_{z=(a+t_w)^-} = 0 \quad \text{for } 0<y<a+t_w \tag{13}$$

Continuity of concentrations and mass flux at the entrance and outlet of the channel are written for both the gas and solid phases. For the gas phase:

$$c = c_0 \quad \text{for } x<0 \tag{14}$$

$$\left.\frac{\partial c}{\partial x}\right|_{x=L^-} = 0 \quad \text{for } y<a, z<a \tag{15}$$

$$\left.\left(\frac{\partial c}{\partial y}+\frac{\partial c}{\partial z}\right)\right|_{y=z} = 0 \quad \text{for } 0<z<a \tag{16}$$

$$\left.\frac{\partial c}{\partial y}\right|_{y=0^+} = 0 \quad \text{for } 0<z<a \tag{17}$$

For the solid phase:

$$\left.\frac{\partial q}{\partial x}\right|_{x=0^+} = 0 \quad \text{for the area of wall facing the inlet stream} \tag{18}$$

$$\left.\frac{\partial q}{\partial x}\right|_{x=L^-} = 0 \quad \text{for the area of wall facing the outlet stream} \tag{19}$$

Tests with different forms of the end boundary conditions were performed to show that they made very little difference to the model predictions. Indeed, the last two boundary conditions could also be described, with no detectable change in predictions, by assuming adsorption at the gas-solid interface in these two locations. This is probably because the surface areas concerned are so small that they have very little influence on the total breakthrough.

The energy balance in the gas phase was written in terms of conduction and convection terms and in the solid phase with conduction only:

$$\rho_g c_{pg} \frac{\partial T_g}{\partial t} - \lambda_g \left(\frac{\partial^2 T_g}{\partial x^2} + \frac{\partial^2 T_g}{\partial y^2} + \frac{\partial^2 T_g}{\partial z^2} \right) + \rho_g c_{pg} u(y,z) \left(\frac{\partial T_g}{\partial x} + \frac{\partial T_g}{\partial y} + \frac{\partial T_g}{\partial z} \right) = 0 \quad (20)$$

$$\rho_s c_{ps} \frac{\partial T_s}{\partial t} - \lambda_s \left(\frac{\partial^2 T_s}{\partial x^2} + \frac{\partial^2 T_s}{\partial y^2} + \frac{\partial^2 T_s}{\partial z^2} \right) = 0 \quad (21)$$

The air density, heat capacity and thermal conductivity were calculated intrinsically by Comsol, the software used to solve the system of equations. The carbon density of 842.2 kg m^{-3} was estimated from the physical characteristics of the monolith and the channel size distribution used to determine the surface area of free flow. The thermal conductivity of the monolith was measured as 18 W m^{-1} K^{-1}.[22] Very little is known of the heat capacity of monolithic carbon. Hence, the heat capacity of carbon[23] of 703 J kg^{-1} K^{-1} was fixed for the modeling.

The energy balance at the wall is described by the following equation:

$$\lambda_s \left. \frac{\partial T_s}{\partial z} \right|_{z=a^+} = \Delta H \frac{d\bar{q}}{dt} + \alpha_g A (T_s - T_0) \quad \text{for } 0<y<a \quad (22)$$

Here, α_g is the heat transfer coefficient of the air, A is the surface area of the wall and T_0 is the inlet temperature of the air stream. In this study, an average value of the heat transfer coefficient was considered to be sufficient and was obtained from the Nusselt number calculated using the Hawthorn[24] correlation for a square channel:

$$\mathrm{Nu} = \frac{h d_{ch}}{\lambda_g} = 2.977 \left(1 + 0.095 \frac{d_{ch}}{L} \mathrm{Re\ Pr} \right)^{0.45} \quad (23)$$

The heat transfer coefficient was, accordingly, found to be 111.4 W m^{-2} K^{-1}.

To complete the energy balance, boundary conditions need to be considered for solid-solid interfaces, for the gas phase and for the solid phase. For the solid-solid interfaces:

$$\left. \frac{\partial T_s}{\partial y} \right|_{y=0^+} = 0 \quad \text{for } a<z<a+t_w \quad (24)$$

$$\left(\frac{\partial T_s}{\partial y} + \frac{\partial T_s}{\partial z} \right) \Big|_{y=z} = 0 \quad \text{for a}<z<a+t_w \quad (25)$$

$$\left. \frac{\partial T_s}{\partial z} \right|_{z=(a+t_w)^-} = 0 \quad \text{for } 0<y<a+t_w \quad (26)$$

For the gas phase:

$$T_g = T_0 \quad \text{for } x<0 \quad (27)$$

$$\left. \frac{\partial T_g}{\partial x} \right|_{x=L^-} = 0 \quad \text{for } y<a, z<a \quad (28)$$

$$\left(\frac{\partial T_g}{\partial y} + \frac{\partial T_g}{\partial z} \right) \Big|_{y=z} = 0 \quad \text{for } 0<z<a \quad (29)$$

$$\left. \frac{\partial T_g}{\partial y} \right|_{y=0^+} = 0 \quad \text{for } 0<z<a \quad (30)$$

For the solid phase:

$$\left. \frac{\partial T_s}{\partial x} \right|_{x=0^+} = 0 \quad \text{for the area of wall facing the inlet stream} \quad (31)$$

$$\left. \frac{\partial T_s}{\partial x} \right|_{x=L^-} = 0 \quad \text{for the area of wall facing the outlet stream} \quad (32)$$

As for the mass balance, the surface areas involved in the last two boundary conditions are so small that they have very little influence on the total energy balance.

About 5 min of computational time on a 3.4 GHz processor PC was required to solve this system of equations using the commercial software Comsol. The average concentration at the outlet of a single monolith channel was obtained by integration across the channel cross-section, as follows

$$c_{ave} = \frac{2}{a^2} \int_0^a \int_0^a c(y,z)\, dy\, dz \quad (33)$$

Results and Discussion

Two approaches to modeling all the channels in a single monolith are now considered. In the first, all channels are assumed to be identical with the nominal dimensions shown in Table 1. This is the basis of the uniform channel model (UCM). In the second, more realistic, approach, the channels are not assumed to be identical in their dimensions. This is the basis of the NUCM in which the pressure drop is considered to be the same across all channels in the monolith; in this case, the model inherently takes the assumption of a uniform pressure distribution in the gas entry chamber. The outlet pressure is uniformly atmospheric. In both approaches, no account is taken of any possible nonuniformities in the axial direction.

Uniform channel model (UCM)

The experimental breakthrough curve for a flow rate of 7 L (STP) min^{-1} is shown in Figure 6. Using the UCM, trial and error was used in the Comsol simulation to find a fixed value of the effective diffusion coefficient which ensured that the predicted breakthrough curve fitted the experimental data, at least in the early part of the breakthrough curve. A value of 9.0×10^{-11} m^2 s^{-1} was found to fit the experiment extremely well up to the point where the dimensionless outlet concentration reached about 0.6 of the feed concentration. Figure 7 shows the gas phase concentration profile for the one-eighth section of the channel (Figure 2) using the UCM. Figure 7 confirms the need to model the gas phase convection-diffusion in three dimensions (as per Eq. 3). The highest gas phase concentration exists, as expected, on the central axis whilst the lowest concentrations exist in the corner.

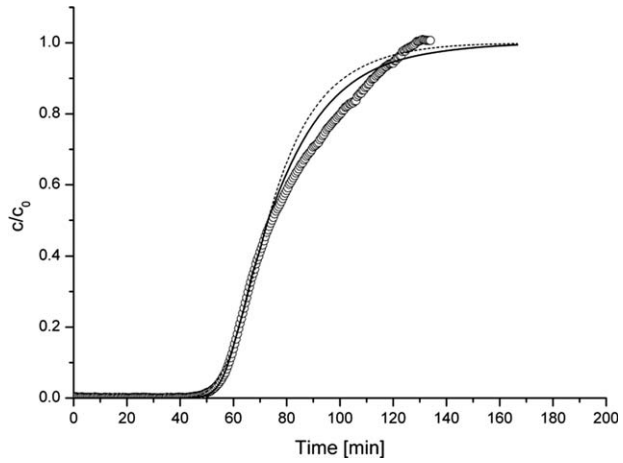

Figure 6. Breakthrough curve of DCM on activated carbon monolith: Experiment at 7 L (STP) min^{-1} (○), single channel model, UCM (—), normal distribution model, NUCM (---).

The effective diffusion coefficient is function of the gas concentration and the temperature. These relationships can be obtained from the kinetic data obtained using the IGA when it is used to obtain the isotherms of adsorption at different temperature. The adsorption isotherms of DCM were measured using small samples taken from the monolith for temperatures of 5, 10 and 20°C. The rate of adsorptive loading was analyzed at gas concentrations up to 5000 ppmv for each temperature resulting in Figure 8.

The slopes and intercepts of the linear fits shown in Figure 8 were also well represented by a straight line when viewed as a function of the temperature. Therefore, the effective diffusion coefficient could be expressed by:

$$D_{\text{eff}} = \text{Intercept}(T_s) + \text{Slope}(T_s) \cdot c \qquad (34)$$

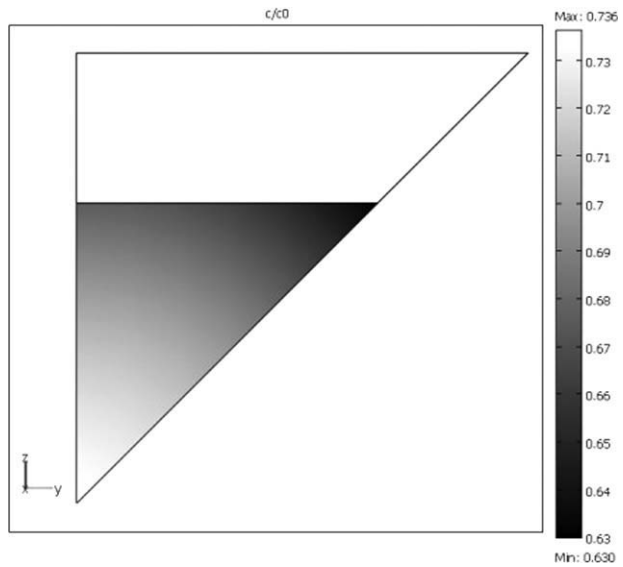

Figure 7. Concentration profile in UCM model at t = 72 min and x = 0.09 m for the 7 L (STP)°min^{-1} experiment at 2000 ppm of DCM.

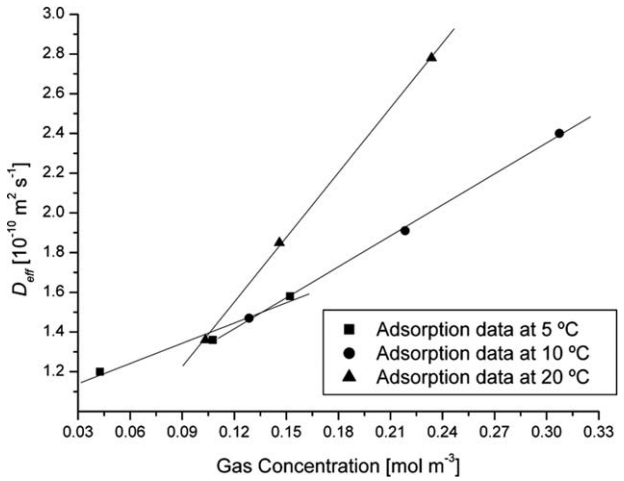

Figure 8. Effective diffusion coefficient of DCM in the carbon monolith estimated from the kinetic data of the adsorption isotherms at three temperatures.

The breakthrough curves obtained using the UCM with the effective diffusion coefficient fixed or expressed using Eq. 34 are almost identical, as shown in Figure 9. However, the run-time required to solve the model using Eq. 34 was almost twice as long as that using a fixed effective diffusion coefficient. For the rest of this work, therefore, the UCM and NUCM have primarily been solved using fixed values for D_{eff}.

In the same way as for the 7 L (STP) min^{-1} experiment, the UCM was used to interpret the experimental data for the other two flow rates shown in Table 2 (5 and 9 L (STP) min^{-1}). For these two flow rates, the effective diffusion coefficients required to obtain excellent fits using the UCM were found to be 4.6×10^{-11} and 1.05×10^{-10} m^2 s^{-1}, respectively. The fits to the experimental data are shown in Figure 10. The fits are excellent up to c/c_0 of around 0.4 and

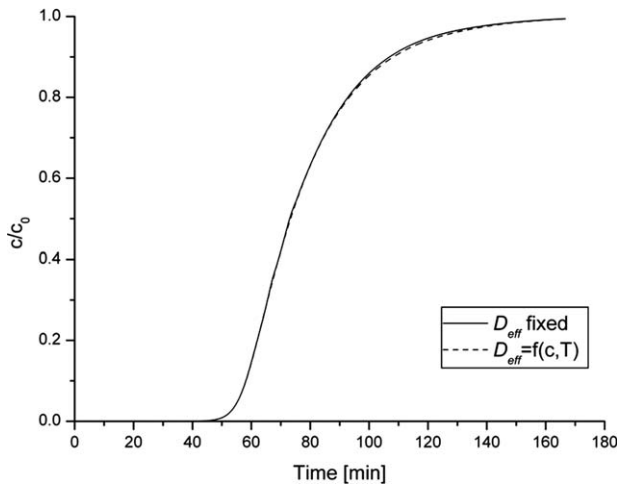

Figure 9. Comparison between breakthrough curves at 7 L (STP) min^{-1} using the UCM with D_{eff} fixed or in function of gas concentration and temperature.

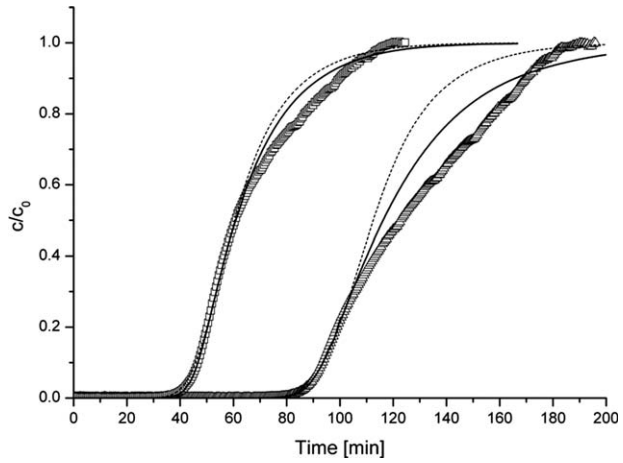

Figure 10. Breakthrough curve of DCM on activated carbon monolith: Experiment at 9 L (STP) min^{-1} (□) and 5 L (STP) min^{-1} (△), single channel model, UCM (—), normal distribution model, NUCM (---).

0.6 for feed flow rates of 5 and 9 L (STP) min^{-1}, respectively.

A slight adjustment needed to be made to the flow rate used in the model to take account of the slightly higher feed concentration used in the run at 7 L (STP) min^{-1} (Table 2). Because the maximum loading of DCM on the monolith cannot depend on the flow rate, a revised flow rate of 4.7 L (STP) min^{-1} was used to fit the experiment at 5 L (STP) min^{-1} to keep the same q_s for all the simulations, and 8.7 L (STP) min^{-1} was used for the breakthrough at 9 L (STP) min^{-1}. These slightly lower flow rates compensate for the slightly lower feed concentrations (Table 1), the variation in flow rate being within the experimental error in its measurement. It is now apparent that by using the UCM there would seem to be a dependency of the effective diffusivity of DCM inside the carbon with the feed flow rate in the gas channel. This is not scientifically possible. Hence, the UCM cannot be used to adequately describe behavior in all the channels in an actual monolith, and so, the NUCM is now considered.

Nonuniform channel model (NUCM)

The channels vary in size and shape as shown in the image of a normal cross-section of the monolith (Figure 11a). Freeware image analysis software (ImageJ) was used to highlight channel cross-sections as shown in Figure 11b. The size of a channel, d, was determined as the side of a square with the same cross-sectional area as the channel image obtained from Figure 11a. Channels near to the edge of the monolith tend to be nonsquare and of smaller cross-sectional area than those in the centre. The average size, d_{ave}, of the channels including the 18 nonsquare channels is 0.688 ± 0.0652 mm whilst d_{ave}, of the channels excluding the 18 nonsquare channels is 0.702 ± 0.0365 mm. For modeling purposes, a channel size of 0.7 mm and a wall thickness of 0.35 mm are used.

The structure of the monolith was described using a Gaussian distribution for the channel size, characterized by an average value and a standard deviation, σ:

$$P(h) = \frac{1}{\sigma\sqrt{2\pi}} \exp\left(-\frac{(h-1)^2}{2\sigma^2}\right) \quad \text{where} \quad h = \frac{d}{d_{ave}} \tag{35}$$

It can be seen from Figure 12 that this distribution provides a good fit to the channel size distribution provided that the nonsquare channels are excluded. The flow through each channel is laminar (Table 2) and hence the single phase pressure drop over a straight channel is given by:

$$\frac{\Delta P}{L} = 4f \frac{(1/2)\rho_g u^2}{d} \tag{36}$$

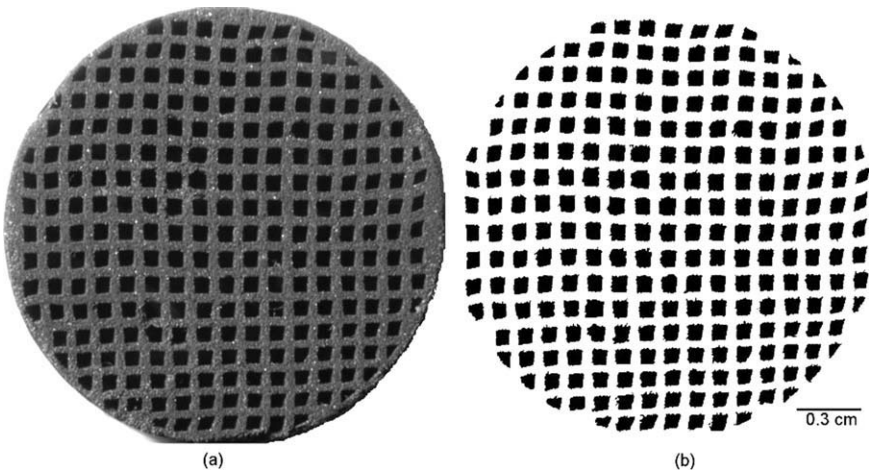

Figure 11. Grey-level image of a square channel monolith (left) reduced to a binary image (right) used to determine its channel size distribution.

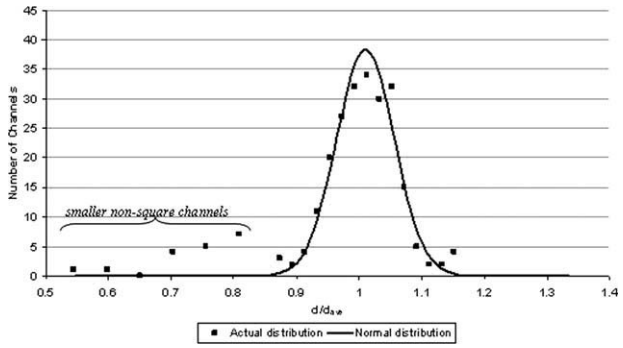

Figure 12. Channel size distribution.

Expressions for the friction factor, f, as a function of the Reynolds number have been established for various duct geometries.[25]

The pressure gradient can then be written as follows:

$$\frac{\Delta P}{L} = \frac{2Cu\mu}{d^2} \tag{37}$$

where C is a constant, and μ is the viscosity of the gas. Now consider any two channels of different size, d_1 and d_2, which have average gas velocities, u_1 and u_2, respectively. The pressure drop across both channels is the same. Hence, the ratio of velocities is related to the ratio of channel sizes by the following equation:

$$\left(\frac{d_1}{d_2}\right)^2 = \frac{u_1}{u_2} \tag{38}$$

The probability function of the normal distribution can then be calculated from the gas velocities in the channels as follows:

$$P(h) = \frac{1}{\sigma\sqrt{2\pi}} \exp\left(-\frac{1}{2\sigma^2}\left(\sqrt{\frac{u}{u_{\text{ave}}}} - 1\right)^2\right) \tag{39}$$

The average velocity, u_{ave}, was determined from the experimental volumetric flowrate. The breakthrough curves for different h values were then obtained for each channel using the UCM as shown in Figure 13 and the average exit concentration over all the channels for the NUCM was then obtained from:

$$c_{\text{cumul}} = \frac{\int_{h_{\min}}^{h_{\max}} c_{\text{ave}}(h)\, u_{\text{ave}}\, h\, P(h)\, dh}{\int_{h_{\min}}^{h_{\max}} u_{\text{ave}}\, h\, P(h)\, dh} \tag{40}$$

The velocity in each channel is given by the expression $u_{\text{ave}}\ h$ and the concentration $c_{\text{ave}}(h)$ represents the averaged outlet concentration for this specific velocity. It can be seen from Figure 13 that the effect of nonuniformities in channel dimensions is to broaden the overall breakthrough curve.

For the NUCM to adequately describe the adsorption properties of the monolith, it is preferable that the unique effective diffusion coefficient D_{eff} for all flow rates is not derived from the experimental breakthrough data but rather from an independent source. The IGA data were therefore used to obtain an independent estimate of the effective diffusion coefficient. By using a linear driving force model[26] to analyze the rate of change in adsorptive loading on the sample in the IGA at a gas-phase concentration of 2000 ppmv, the effective diffusion coefficient of DCM was found to be $\sim 1.36 \times 10^{-10}$ m^2 s^{-1}. This value compares reasonably well with the effective diffusion coefficient of 1.7×10^{-10} m^2 s^{-1} required to fit the experimental data for a flow of 7 L (STP) min^{-1} using the NUCM as shown in Figure 6. The channel size distribution used in the NUCM was broader ($\sigma = 0.046$ mm) than the distribution observed when considering only the well-formed square channels ($\sigma = 0.0365$ mm). As can be seen from Figure 6, the NUCM leads to a slightly different completion of the breakthrough curve than either the experimental data or the UCM. One reason for this is that the effective diffusion coefficient used in the NUCM is somewhat higher than that obtained by back-calculation using the UCM. In the NUCM, the air flow is slower in the smaller channels. Thus, the full breakthrough has not been reached in such channels explaining the slightly different loadings predicted by the models. The channel outlet temperatures were not measured during the breakthrough experiments and could not be compared with the predictions by both models shown in Figure 14. The heat released during the adsorption would limit the adsorption capacity in the solid. After the breakthrough front has passed a certain point in the channel, the temperature would decrease allowing for further VOC uptake to take place. This would slow down the uptake after the breakthrough has been reached compared with an isothermal model. The temperature front during the breakthrough in the larger channels moves faster than in the smaller channels. Furthermore, the higher VOC flow through the larger channels releases a greater amount of heat explaining the sharper increase and the higher maximum in the outlet temperature (Figure 14). The amount of released heat predicted by both models should be similar. Thus, the outlet

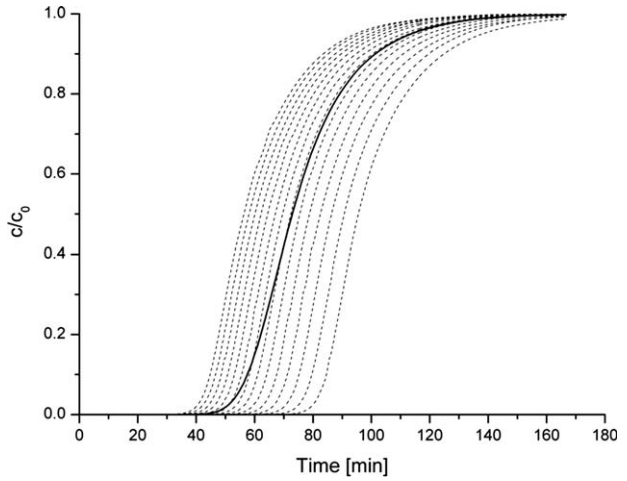

Figure 13. Breakthrough curves for each *h* value (dashed lines) and cumulative breakthrough for the monolith (full line).

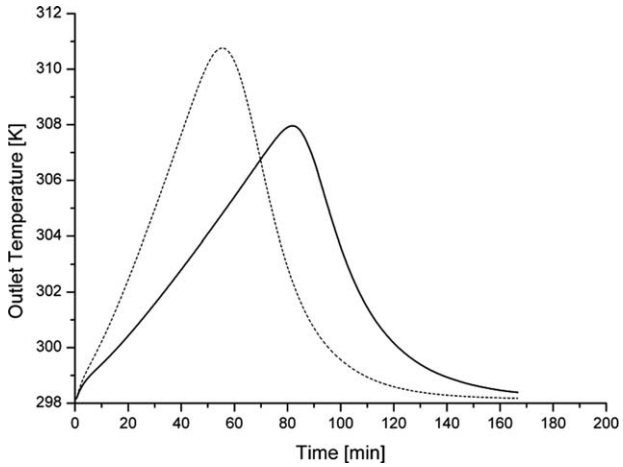

Figure 14. Channels outlet temperatures predicted by the UCM (__) and the NUCM (---) models.

temperature decreases faster past its maximum with the NUCM than with the UCM.

To test the robustness of the NUCM, the same normal distribution and the same effective diffusion coefficient were then used to model the results for the other two feed flow rates of 5 and 9 L (STP) min^{-1}. The simulations are compared with the experimental data in Figure 10. As for the case with a feed flow rate of 7 L (STP) min^{-1}, the first part of the experimental breakthrough curve for both feed flow rates is very well represented by the nonuniform flow model, whilst at higher concentrations in the breakthrough curve, the diffusion in the solid predicted by the model seems to be too fast to explain the tail observed in the experimental data. Nevertheless, the fact that the early part of the breakthrough curve with different feed flow rates can be modeled by a single, independently obtained, effective diffusion coefficient means that the NUCM is scientifically better than the UCM and augurs very well for future refinements.

Neither channel model (UCM or NUCM) is able to fit the complete breakthrough of DCM (at high values of dimensionless concentration) indicating that one or more of the assumptions made in them are invalid. Whilst the UCM appears to be better in fitting the experimental breakthrough curves (Figures 6 and 10), this model is fundamentally flawed in that the effective diffusion coefficient within the solid phase has to be varied with the gas flow rate in the monolith channels to obtain good matches between simulated and experimental results. This is not scientifically feasible. The NUCM is not fundamentally flawed in this respect and is far superior scientifically since the effective diffusion coefficient has been obtained from an independent experiment using the IGA. As for the UCM, the dependency of the effective diffusion coefficient on both gas concentration and temperature did not improve significantly the matching of simulated and experimental breakthrough curves at high dimensionless concentrations. It is possible therefore that the properties of the pores within the monolith wall may not be uniform and could vary with position. Indeed, the shapes of the experimental breakthrough curves shown in Figures 6 and 10 are interesting in this respect, because they do not show the normal shape of a breakthrough curve with a single, dilute adsorptive. Whilst only a few breakthrough curves are shown in this article, the change in shape which can be seen in Figures 6 and 10 at a dimensionless concentration in the range of 0.4 to 0.6 is typical of many others obtained with the MAST Carbon monolith.[22]

Conclusions

Two approaches have been compared in the modeling of experimental breakthrough curves of a volatile organic compound on a binder-less activated carbon monolith. When all channels are assumed to be identical (the UCM), relatively low effective diffusion coefficients in the solid are required to model the experimental data with reasonable success. The need to vary the effective diffusion coefficient with feed flow rate, and hence with channel gas velocity, is a fundamental weakness of this simpler model and directs research away from the commonly made assumption that all channels behave the same. In the new NUCM, a normal distribution of channel sizes is used to model the actual monolithic structure. It is then found that a single independently obtained effective diffusion coefficient can be used with reasonable success in this NUCM for all three feed flow rates studied in this research. The characteristics of the monolith (VOC adsorption properties, channel and wall thickness dimensions, effective diffusivity, etc.) as measured independently can be used as parameters in the NUCM model to represent accurately the experimental data up to dimensionless breakthrough concentrations of about 0.4–0.6.

Diffusion into the solid with the NUCM, however, is still too fast to simulate correctly the tailing observed with the experimental breakthrough curves at high values of c/c_0. Accordingly, further improvements are required to the NUCM by possibly incorporating the anisotropic nature of the carbon structure.

Acknowledgments

The authors are grateful to the Engineering and Physical Sciences Research Council (EPSRC) for funding this work as part of a Joint Grant Scheme with the Defence Science and Technology Laboratory, Porton Down, UK, under grant reference GR/S55804/01. The support of MAST Carbon Technology in supplying the research sample of activated carbon monolith is gratefully acknowledged.

Notation

A = wall surface area (m^2)
a = half channel size (mm)
a^- = position at the gas–solid interface in the gas phase
a^+ = position at the gas–solid interface in the solid phase
b = affinity coefficient (Pa^{-1})
b_0 = pre-exponential factor of affinity coefficient (Pa^{-1})
c = gas phase concentration (mol m^{-3})
c_0 = feed gas concentration (mol m^{-3})
c_{ave} = average concentration at the outlet of a monolith channel (mol m^{-3})
c_{cumul} = average concentration over all the channels in the distributed channel model (mol m^{-3})
c_{pg} = heat capacity of the gas (J kg^{-1} K^{-1})
c_{ps} = heat capacity of carbon (J kg^{-1} K^{-1})
d = channel size (m)
d_{ave} = average channel size in Gaussian distribution (mm)
d_{ch} = nominal channel size (mm)
D_{eff} = effective diffusion coefficient (m^2 s^{-1})
d_m = monolith overall diameter (cm)

D_M = molecular diffusion coefficient ($m^2\ s^{-1}$)
e = nominal wall thickness (mm)
f = friction factor
h = dimensionless channel size
ΔH = isosteric heat of adsorption (kJ mol^{-1})
k = mass transfer coefficient in LDF equation 5 (s^{-1})
L_m = monolith overall length (mm)
p = partial pressure of DCM (Pa)
$P(h)$ = probability density function of normal distribution
ΔP = pressure drop over a straight channel (Pa)
q = adsorbate loading in carbon wall (mol m^{-3})
$\overline{q}$ = mean adsorbate loading (mol m^{-3})
q^* = adsorbate loading in equilibrium with fluid phase (mol m^{-3})
q_{max} = adsorption capacity of the carbon (mol m^{-3})
R = molar gas constant (= 8.314 J $mol^{-1}\ K^{-1}$)
T_0 = gas stream inlet temperature (K)
T_g = gas stream temperature (K)
T_s = carbon wall temperature (K)
t_w = half wall thickness (mm)
u = gas channel velocity (m s^{-1})
u_{ave} = average channel gas velocity (m s^{-1})

Greek letters

α_g = Heat transfer coefficient of the air (W $m^{-2}\ K^{-1}$)
ε = Fractional free cross-section
λ_g = gas stream thermal conductivity (W $m^{-1}\ K^{-1}$)
λ_s = carbon monolith thermal conductivity (W $m^{-1}\ K^{-1}$)
μ = gas viscosity (Pa s)
ρ_g = gas density (kg m^{-3})
ρ_s = carbon density (kg m^{-3})
σ = standard deviation of Gaussian distribution of channel sizes (mm)

Literature Cited

1. Crezee E, Tennison SR, Rawlinson AP, Place RN, Crittenden BD, Perera SP. Electrically regenerable carbon monolithic adsorption system for the recovery and recycle of volatile organic chemicals (VOCs). Paper Presented at 7th World Congress of Chemical Engineering, July 10–14, 2005, Glasgow, United Kingdom.
2. Vergunst T, Kapteijn F, Moulijn JA. Preparation of carbon-coated monolithic supports. *Carbon*. 2002;40:1891–1902.
3. Garcia-Bordeje E, Kapteijn F, Moulijn JA. Preparation and characterisation of carbon-coated monoliths for catalyst supports. *Carbon*. 2002;40:1079–1088.
4. De Lathouder KM, Lozano-Castello A, Linares-Solano A, Wallin SA, Kapteijn F, Moulijn JA. Carbon-ceramic composites for enzyme immobilization. *Microporous Mesoporous Mater*. 2007;99:216–223.
5. Barannik GB. Composite honeycomb monoliths. *React Kinet Catal Lett*. 1997;60:291–296.
6. Yates M, Blanco J, Avila P, Martin MP. Honeycomb monoliths of activated carbons for effluent gas purification. *Microporous Mesoporous Mater*. 2000;37:201–208.
7. Tennison SR. Phenolic resin-derived activated carbons. *Appl Catal A*. 1998;173:289–311.
8. Tennison SR, Blackburn AJ, Rawlinson AP, Place RN, Crittenden BD, Fair S. Electrically regenerable monolithic adsorption system for the recovery and recycle of solvent vapours. Paper Presented at: Proc AIChE Spring Meeting, 2001, Houston.
9. Crittenden BD, Patton A, Jouin C, Perera SP, Tennison S, Botas Echevarria JA. Carbon monoliths: a comparison with granular materials. *Adsorption*. 2005;11(suppl 1):537–541.
10. Lapkin A, Joyce L, Crittenden BD. A framework for evaluating the "greenness" of chemical processes, a case study of a novel VOC recovery technology. *Environ Sci Technol*. 2004;38:5815–5823.
11. Crittenden BD, Perera SP, Mays TJ, Camus O, Tennison SR. Monolithic adsorbents in sustainable development. Paper Presented at: 7th World Congress of Chemical Engineering, 2005, Glasgow, United Kingdom.
12. Golay MJE. *Theory of chromatography in open and coated tubular columns with round and rectangular cross-sections*. In: Desty DH, editor. *Gas Chromatography*. New York: Academic Press, 1958: 36–55.
13. Ahn H, Brandani S. Analysis of breakthrough dynamics in rectangular channels of arbitrary aspect ratio. *AIChE J*. 2005;51:1980–1989.
14. Ahn H, Brandani S. Dynamics of carbon dioxide breakthrough in a carbon monolith over a wide concentration range. *Adsorption*. 2005; 11:473–477.
15. van Gulijk C, Linders MJG, Valdés-Solís T, Kapteijn F. Intrinsic channel maldistribution in monolithic catalyst support structures. *Chem Eng J*. 2005;109:89–96.
16. Grande CA, Cavenati S, Barcia P, Hammer J, Fritz HG, Rodrigues AE. Adsorption of propane and propylene in zeolite 4A honeycomb monolith. *Chem Eng Sci* 2006;61:3053–3067.
17. Perdana I, Creaser D, Bendiyasa IM, Rochmadi, Tyoso BW. Modelling NOx adsorption in a thin NaZSM-5 film supported on a cordierite monolith. *Chem Eng Sci* 2007;62:3882–3893.
18. Petkovska M, Antov-Bozalo D, Markovic A, Sullivan P. Multiphysics modeling of electric-swing adsorption system with in-vessel condensation. *Adsorpt J Int Adsorpt Soc*. 2007;13:357–372.
19. Cornish RJ. Flow in a pipe of rectangular cross-section. *Proc Roy Soc Lon A Math Phys Sci* 1928;120:691–700.
20. Fuller EN, Schettler PD, Giddings JC. A new method for prediction of binary gas phase diffusion coefficient. *Ind Eng Chem*. 1966;58:19–27.
21. Patton A, Crittenden BD, Perera SP. Use of the linear driving force approximation to guide the design of monolithic adsorbents. *Chem Eng Res Des*. 2004;82:999–1009.
22. Sanchez-Liarte F. Performance of electrically regenerable monolithic adsorbents for VOC control. PhD Thesis Chemical Engineering, University of Bath, Bath, 2009.
23. Perry RH, Green DW. *Specific Heats of Miscellaneous Materials. Perry's Chemical Engineers' Book*, 7th ed. New York: McGraw-Hill, 1997:2–186.
24. Hawthorn RD. Afterburner Catalysts-effects of Heat and Mass Transfer between Gas and Catalyst Surface. *AIChE Symp Ser*. 1974;70:428–438.
25. Kakaç S, Shah RK, Aung W, editors. *Handbook of Single-Phase Convective Heat Transfer*. New York: Wiley, 1987.
26. Chagger HK, Ndaji FE, Sykes ML, Thomas KM. Kinetics of adsorption and diffusional characteristics of carbon molecular sieves. *Carbon*. 1995;33:1405–1411.

Manuscript received Feb. 5, 2010, and revision received Jun. 1, 2010.